Available online at www.sciencedirect.com
ScienceDirect
Journal of Nuclear Materials 367–370 (2007) 428–433
journal of nuclear materials
www.elsevier.com/locate/jnucmat

Helium effects on mechanical properties and microstructure of high fluence ion-irradiated RAFM steel

H. Ogiwara [a,b,*], A. Kohyama [b], H. Tanigawa [c], H. Sakasegawa [d]

[a] Graduate School of Energy Science, Kyoto University, Gokasho, Uji, Kyoto 611-0011, Japan
[b] Institute of Advanced Energy, Kyoto University, Gokasho, Uji, Kyoto 611-0011, Japan
[c] Naka Fusion Institute, Japan Atomic Energy Agency, Tokai, Naka, Ibaraki 319-1195, Japan
[d] Oarai Research and Development Center, Japan Atomic Energy Agency, Narita, Oarai, Ibaraki 311-1393, Japan

Abstract

Reduced-activation ferritic/martensitic steels, RAFS, are leading candidates for the blanket and first wall of fusion reactors, and effects of displacement damage and helium production on mechanical properties and microstructures are important to these applications. Because it is the most effective way to obtain systematic and accurate information about microstructural response under fusion environment, single-(Fe^{3+}) and dual-($Fe^{3+} + He^{+}$) irradiations were performed followed by TEM observation and nano-indentation hardness measurement. Dual-ion irradiation at 420 °C induced finer defect clusters compared to single-ion irradiation. These fine defect clusters caused large differences in the hardness increase between these irradiations. TEM analysis clarified that radiation induced precipitates were MX precipitates (M: Ta, W). Small defects invisible to TEM possibly caused the large increase in hardness, in addition to the hardness increment produced by radiation induced MX. In this work, radiation hardening and microstructural evolution accompanied by the synergistic effects to high fluences are discussed.

1. Introduction

Reduced-activation ferritic/martensitic steel, RAFS are leading candidates for the blanket and first wall of fusion reactors because of their excellent mechanical properties, microstructural stability and swelling resistance under the fission neutron irradiation environment [1–4]. The irradiation effects of microstructural defects and gaseous transmutation species may affect the microstructural development in fusion environment, and the mechanisms have not sufficiently evaluated. Because it is the most effective way to obtain systematic and accurate information about microstructural response in a fusion environment, single-(Fe^{3+}) and dual-($Fe^{3+} + He^{+}$) ion irradiations were performed followed by TEM observation and nano-indentation. For reference, ion-irradiated F82H to high He/dpa at 633 K caused the radiation hardening accompanied by the formation of black dot defects, which were probably dislocation loops, radiation induced precipitates and nano-voids [5]. Under neutron

* Corresponding author. Address: Institute of Advanced Energy, Kyoto University, Gokasho, Uji, Kyoto 611-0011, Japan. Tel.: +81 774 38 3466; fax: +81 774 38 3467.
E-mail address: hiroyuki_ogiwara@iae.kyoto-u.ac.jp (H. Ogiwara).

0022-3115/$ - see front matter © 2007 Elsevier B.V. All rights reserved.
doi:10.1016/j.jnucmat.2007.03.120

irradiation, the radiation hardening caused by irradiation-induced dislocation loops and precipitates changes occurred at irradiation temperatures up to 420 °C [2]. Radiation induced precipitates (RIP) M_6C, Laves phase were identified under FFTF neutron irradiation [6], and one of the issues is to understand the hardening mechanism of these RIP in a fusion neutron environment. The objectives of this work are to clarify the helium effects on radiation hardening and the mechanism reflected by microstructural evolution, such as dislocation evolution and RIP formation.

2. Experimental procedure

The used material was a RAFS, JLF-1, from the second large heat (Fe–9Cr–2W–0.2V–0.08Ta) [7]. Heat treatments were normalized at 1050 °C for 1 h in air followed by air cooling (AC), followed by tempering at 780 °C for 1 h and followed by AC. Before the ion irradiation experiments, 3 mm diameter TEM disks were mechanically polished to about 0.25 mm thick. Finally, electrolytic polishing was carried out at 4 °C, 20 V.

A dual-ion irradiation technique was used for this work because this technique is able to control the displacement damage and precise control of the helium-to-dpa (displacement per atom) ratio. The single-ion irradiation used 6.4 MeV Fe^{3+} ions. In the case of dual-ion irradiations, 6.4 MeV Fe^{3+} ions and energy-degraded 1.0 MeV He^{+} ions were simultaneously used. The implantation energy of helium ions was reduced and varied from 200 keV to 1.0 MeV by using the energy degrader. JLF-1 steels were irradiated up to 60 dpa at 420 °C. The displacement damage rate and helium injection rate were 1.0×10^{-3} dpa/s and 15 appm He/dpa at the depth of 0.85 μm from the specimen surface, respectively. These calculations were performed by TRIM code [8] assuming an average displacement threshold energy of 40 eV. The specimen temperature was continuously monitored by the infrared thermal vision (Nikon Thermal Vision LAIRD 3ASH-K). The specimen temperature during irradiation was maintained within ±10 °C of nominal temperature for the entire period of irradiation experiments.

Nano-indentation measurements were performed using the Elionix Inc. (Tokyo, Japan) Model ENT-1100a. A Berkovich indenter was used, and the tip truncation was calibrated using fused silica as a reference specimen. Analysis of the tip calibration and the calculation of hardness were conducted by the method used by Oliver and Pharr [9]. Irradiated specimens were prepared by electrochemically removing about 500 nm from the ion bombarded side. Removed depths were measured with the Micromap™ interferometric optical surface profiling system (Micromap Inc., Tucson, USA). Maximum penetration depths of nano-indentation were less than 200 nm at the peak load for all the specimens.

Thin foils for TEM examination were prepared with a focused ion beam (FIB) micro-processing device. TEM observations were performed using 200 kV JEOL-2010 and JEOL-2200FS microscopes. Determination of thin-foil thicknesses was performed by Convergent beam electron diffraction (CBED) technique.

3. Results

3.1. Dose dependence of radiation hardening

Fig. 1 shows the dose dependence of micro-hardness changes of JLF-1 steel, ΔH ($=H_{\mathrm{Irra.}} - H_{\mathrm{Unirra.}}$) by single- and dual-ion irradiation up to 60 dpa at 420 °C. ΔH increased with increasing dose. Dual-ion irradiation to 60 dpa resulted in the large increase in ΔH. Differences in ΔH in radiation hardening between single- and dual-ion irradiation might indicate the microstructural evolution, dislocation evolution and RIP. To identify the mechanisms accompanied by the microstructural evolution, TEM observation were carried out.

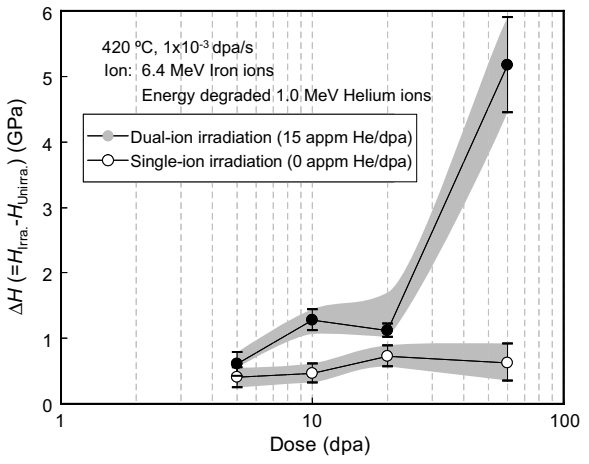

Fig. 1. Dose dependence of radiation hardening up to 60 dpa at 420 °C.

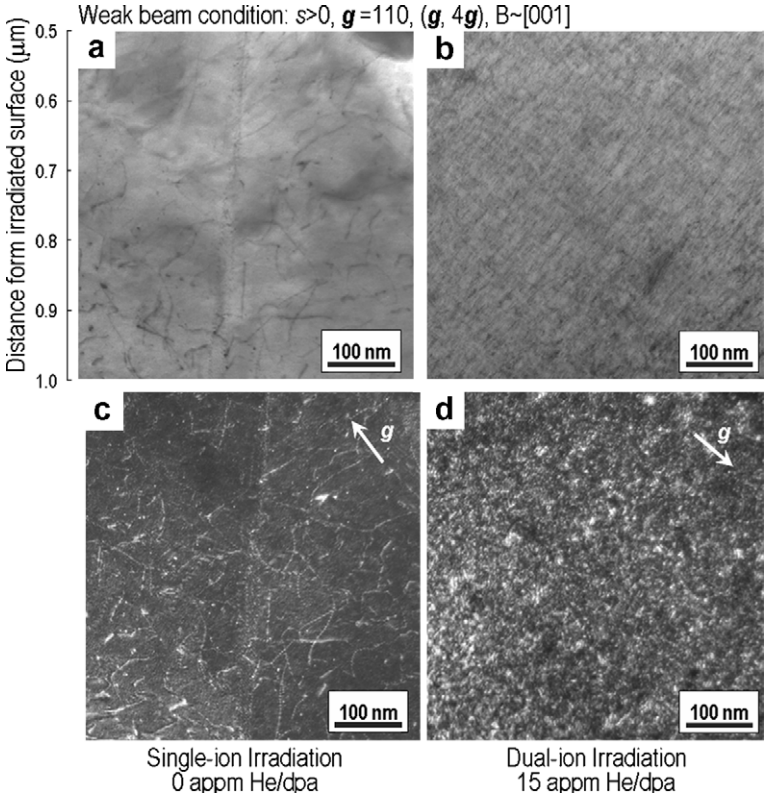

Fig. 2. Bright field images of (a) single- and (b) dual-ion irradiated JLF-1 steel up to 60 dpa at 420 °C, and dislocation images of (c) single- and (d) dual-ion irradiated JLF-1. Weak beam condition: $s > 0$, $\boldsymbol{g} = 1\,1\,0$ ($\boldsymbol{g}$, $4\boldsymbol{g}$), B $\sim$ [0 0 1].

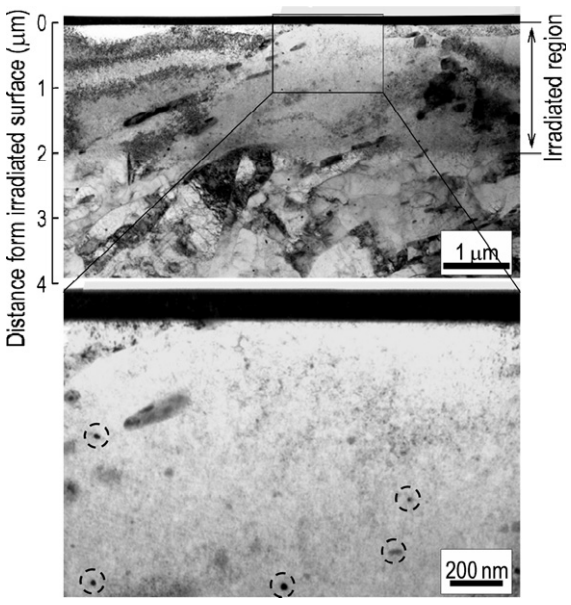

Fig. 3. Black dots in dual-ion irradiated region.

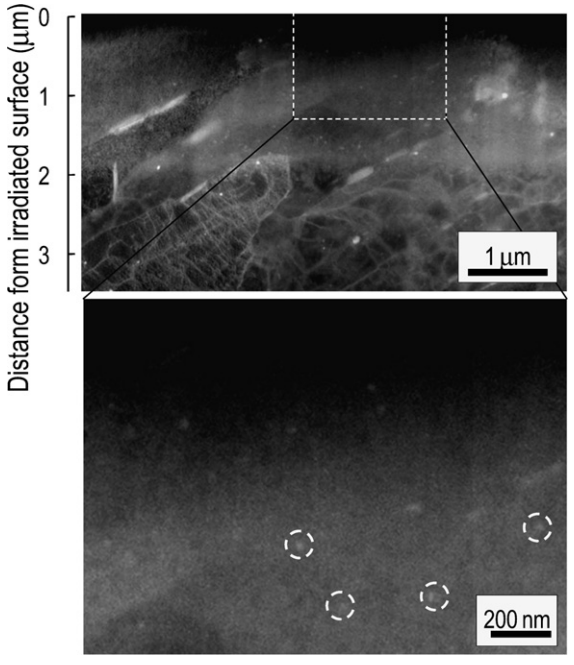

Fig. 4. *Z* contrast images obtained using a high-angle annular dark field detector in a STEM.

3.2. Microstructural evolution

3.2.1. Dislocation evolution

Fig. 2 shows bright field images of (a) single- and (b) dual-ion irradiated JLF-1 steel up to 60 dpa at 420 °C, respectively. No voids were observed under single- and dual-ion irradiation, however, they were observed at 470 °C [10]. Fig. 2 also shows dislocation images of (c) single- and (d) dual-ion irradiated JLF-1. Dislocation structures under single-ion irradiation consisted of the dislocation loops and dislocation lines. Dual-ion irradiation caused finer dislocation loops than single-ion irradiation. Mean diameters of the dislocation loops in single- and dual-ion irradiation were estimated to be 5.1 nm and 6.6 nm, respectively. Densities of dislocation loops in single- and dual-ion irradiation were 8.4×10^{22} m^{-3} and 1.4×10^{23} m^{-3}, respectively.

Radiation-hardening due to these microstructural features was calculated using the dispersed barrier hardening model; $\Delta\sigma = \alpha\mu b(Nd)^{0.5}$, where α is a parameter that describes the strength of the obstacle, μ is the shear modulus and b is the Burgers vector. The hardness changes were calculated by using the equation $\Delta H = 3\Delta\sigma$ and the following parameters: $\alpha = 0.3$ for dislocation loops and other defect clusters [11], $\mu = 8.0 \times 10^{1}$ GPa and $b = 2.68 \times 10^{-1}$ nm [12]. The estimated hardening produced by the formation of dislocation loops, ΔH, in single- and dual-ion irradiation were 6.6×10^{-1} GPa and 5.6×10^{-1} GPa, respectively. Measured hardness of dual-ion irradiation to 60 dpa is

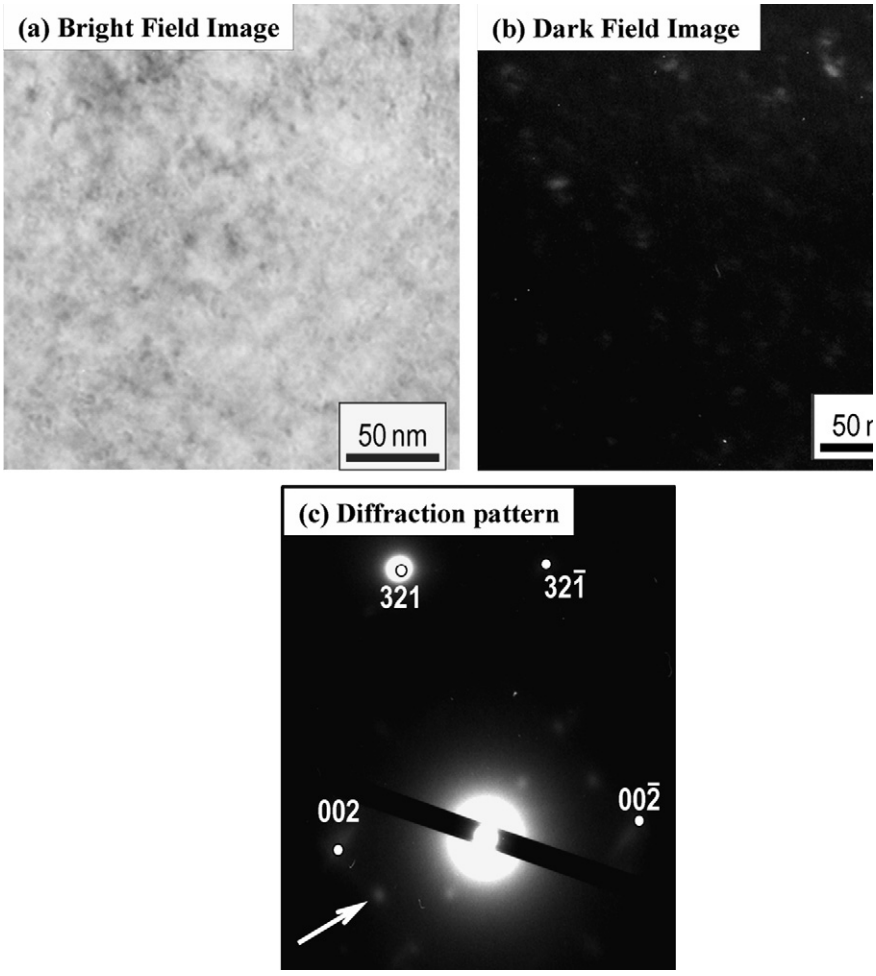

Fig. 5. (a) Bright field image, (b) dark field image and (c) diffraction patterns of dual-ion irradiated JFL-1 steel up to 60 dpa at 420 °C. Dark field image was indicated by the arrow in the corresponding diffraction patterns from precipitates.

larger than the calculated value. This difference between measured and calculated ΔH was 3.8 GPa. The major source of the radiation induced hardening is not the Orowan type loop hardening but other mechanisms.

3.2.2. Radiation induced precipitate

Fig. 3 shows the bright field images under dual-ion irradiation to 60 dpa at 420 °C. Black-spot images were observed in the dual-ion irradiated region, however they were not observed in the unirradiated JLF-1. Dual-ion irradiation introduced the black-spot images due to the formation of nano-void, RIP and dislocation loops.

Z contrast images obtained using a high-angle annular dark field detector in a STEM are shown for the same specimen in Fig. 4. Z contrast imaging is a useful way of getting compositional information from complex structures. The inelastic scattering power of an atom is proportional to the square of its atomic number Z; atoms with higher Z appear brighter. These dot-like spots in Fig. 4 are probably RIP, where these precipitates include Ta, W.

Fig. 5 shows (a) bright field image and (b) dark field image using the precipitate diffraction spots indicated by the arrow in (c). Again, this in the same specimen as in Figs. 3 and 4. The $0\,0\,2$, $0\,0\,\bar{2}$, $3\,2\,1$ and $3\,2\,\bar{1}$ reflections are from the matrix. Assuming that its precipitates were probably MX precipitates, the calculated plane spacing d_{110} with diffraction pattern in Fig. 5(c) was 3.1×10^{-1} nm, and the lattice parameter was $a_0 = 4.4\times10^{-1}$ nm. Mean diameter and number density of RIP were estimated to be 7.3 nm and $4.8\times10^{21}\,\mathrm{m}^{-3}$, respectively. The estimated hardening accompanied by the formation of RIP was 5.3×10^{-1} GPa, using the parameter: $\alpha = 1$ for RIP. Dislocation structures were composed of Burger's vectors of $1/2\langle1\,1\,1\rangle$ and $\langle1\,0\,0\rangle$, but the two types could not be distinguished. It is thought that point defects (vacancies including helium atoms) did not result in helium-assisted void growth at 420 °C, but caused radiation hardening.

4. Discussion

The important issue is o understand the mechanism of material behaviors under a fusion neutron environment. Among the radiation effect of the dual-ion irradiated JLF-1 are the introduction of finer defect clusters than single-ion, and a large increase in hardening. It appears that the presence of helium significantly enhanced irradiation hardening to 60 dpa at 420 °C. Radiation-hardening accompanied by the formation of dislocation loops and RIP was calculated using the dispersed barrier hardening model. However, invisible small defects not resolved with TEM possibly produced the large increase in hardness in addition to the radiation induced MX precipitates. The potential roles of radiation induced MX precipitates and/or invisible defect clusters with TEM in radiation hardening mechanism in the fusion environment (helium effect) up to high fluences requires further study.

5. Conclusion

For the case of JLF-1 irradiated at 420 °C, dual-ion irradiation introduced finer defect clusters than single-ion irradiation, where a larger amount of hardening was measured for the case of dual-ion. TEM analysis suggested that the RIPs are probably MX precipitates (M: Ta, W). These fine precipitates were interpreted to be the origin of the large hardening. The quantitative analysis of the hardening may require the contribution of small precipitates and/or defect clusters with the smaller size than the detection limit for TEM. This work suggests that potential large radiation hardening may be caused by very fine precipitates and/or defect clusters introduced in a fusion environment.

Acknowledgements

This research was partially supported by the Ministry of Education, Science, Sports and Culture, Grant-in-Aid for JSPS Fellows.

References

[1] Y. Kohno, D.S. Gelles, A. Kohyama, M. Tamura, A. Hishinuma, J. Nucl. Mater. 191–194 (1992) 868.
[2] A. Kohyama, A. Hishinuma, D.S. Gelles, R.L. Klueh, W. Dietz, K. Ehrlich, J. Nucl. Mater. 233–237 (1996) 138.
[3] A. Hishinuma, A. Kohyama, R.L. Klueh, D.S. Gelles, W. Dietz, K. Ehrlich, J. Nucl. Mater. 258–263 (1998) 193.
[4] S. Jitsukawa, A. Kimura, A. Kohyama, R.L. Klueh, A.A. Tavassoli, B. van der Schaaf, G.R. Odette, J.W. Rensman, M. Victoria, C. Petersen, J. Nucl. Mater. 329–333 (2004) 39.
[5] M. Ando, E. Wakai, T. Sawai, H. Tanigawa, K. Furuya, S. Jitsukawa, H. Takeuchi, K. Oka, S. Ohnuki, A. Kohyama, J. Nucl. Mater. 329–333 (2004) 1137.
[6] T. Shibayama, A. Kimura, H. Kayano, J. Nucl. Mater. 233–237 (1996) 270.
[7] A. Kohyama, Y. Kohno, M. Kuroda, A. Kimura, F. Wan, J. Nucl. Mater. 258–263 (1998) 1319.

[8] J.F. Ziegler, J.P. Biersack, U. Littmark, The Stopping and Range of Ions in Solids, Pergamon, New York, 1985.
[9] W.C. Oliver, G.M. Pharr, J. Mater. Res. 7 (1992) 1564.
[10] H. Ogiwara, H. Sakasegawa, H. Tanigawa, M. Ando, Y. Katoh, A. Kohyama, J. Nucl. Mater. 307–311 (2002) 299.
[11] E. Wakai, A. Hishinuma, K. Usami, Y. Kato, S. Takaki, K. Abiko, Mater. Trans. 41 (2000) 1180.
[12] R. Schaeublin, D. Gelles, M. Victoria, J. Nucl. Mater. 307–311 (2002) 197.